National Aeronautics and Space Administration

Magnetometer Technology Development for the ARTEMIS Initiative

Principal Investigator: Carol Raymond (410); Co-Investigators: Corey Cochrane (389), Neil Murphy (326), David Pierce (326), Nan Yu (332)

Program: FY21 R&TD Strategic Initiative **Strategic Focus Area: Architecture for Thermal Enclosure of Moon Instrument Suites**

Objectives

The overall objective is to develop and validate an implementation strategy to perform long-term magnetic field measurements on the lunar surface using existing vector helium magnetometer technology (VHM), including a boom and cabling uniquely suited for the environment, and integration into the ARTEMIS-T thermal enclosure. Our focus is on the specific needs of lunar science missions, particularly those that use commercial spacecraft. In pursuit of this objective, we plan to:

- *develop a set of measurement and accommodation requirements driven by potential lunar science objectives*
- *extend our previous assessment of the state-of-the-art in compact, stable, and precise magnetometers, judging their potential to satisfy these requirements, and the timescale for any necessary technology development*
- *review current magnetometer technology to verify that the VHM is the best system to meet the science requirements for long-term magnetic field monitoring on the lunar surface.*
- *explore the potential for new technology sensors to support the removal of lander contaminate magnetic fields*

Background

Magnetic field measurements are required to address several key lunar science goals including: (1) magnetic sounding to determine the moon's internal electrical conductivity profile; (2) understanding the effects of the solar wind and Earth's magnetotail plasma on surface composition; (3) determining if OH depletion seen in lunar swirls is the result of strong magnetic field anomalies (mini-magnetospheres) shielding the surface from the solar wind; and (4) determining the origin of the lunar crust magnetic field. Probing the internal conductivity structure drives requirements, as continual monitoring of the lunar induction field for more than one year is needed, with a magnetometer accuracy of <100 pT at a cadence of 0.1s. In addition, to facilitate meaningful comparison between multiple magnetometers, and ensure accuracy of <100 pT considering other noise sources, the stability of the magnetometer needs to be < 25 pT. The VHM is capable of meeting these requirements, perhaps uniquely.

Significance/Benefits to JPL and NASA

This work provides JPL with a competitive advantage in responding to future NASA Announcements of Opportunity for *Payloads and Research Investigations on the Surface of the Moon* (PRISM). Demonstrating the capability to deploy the high-heritage VHM (Figure 1) along with a seismometer housed within the ARTEMIS-T enclosure creates an alternate architecture to achieve the goals of the Lunar Geophysical Network called for in the New Frontiers Program but utilizing the existing CLPS landers.

Figure 1. The VHM awaiting launch on the CubeSat for Solar Particles (CuSP) mission is a fourth generation version of the JPL compact laser-pumped helium magnetometer

National Aeronautics and Space Administration

Jet Propulsion Laboratory
California Institute of Technology
Pasadena, California

www.nasa.gov

Approach and Results

Results were achieved that:

- *demonstrate a robust approach to operations over the wide temperature range (~95K to 390K) of the lunar diurnal cycle*
- *characterize noise sources and demonstrate system performance*
- *retire risks associated with lunar deployment*

Our approach in FY21 was to 1) utilize a newly constructed laboratory laser/optical fiber testbed to characterize and mitigate system noise resulting from environmental stresses on the optical fiber, and the impact of the phase variations on the phase lock loop performance; 2) create a notional lander magnetic field model and perform modeling to determine the required boom length to meet the science performance requirement of <100 pT and to quantify the trade between the number of sensors and boom length; 3) evaluate options for the deployable boom and cable routing and develop interface requirements for integration with the ARTEMIS-T enclosure. Results are summarized below.

Laser/Fiber Testbed. The testbed (Figure 2) consists of a 1083 nm distributed Bragg laser reflector laser diode and controller, with a Fabry Perot spectrometer, polarimeter, and laser power meter controlled via LabView code. The laser output was coupled to a 2 x 2 fiber splitter, and which could be used to feed any two of the measuring devices. By feeding one output of the splitter via an additional length of fiber, back to one of the splitter inputs it operates as a delay loop. The delay loop was used to scramble polarization in an attempt to reduce phase noise due to ambient temperature variations. Under varying mechanical stress on the fiber, polarization with and without a delay loop was measured. An example is shown in Figure 3. The two plots show the effectiveness of polarization scrambling on reducing polarization variations caused by variable mechanical stress on the fiber. Testing confirmed that while polarization is not completely scrambled, variations seem to be stochastic, yielding a low, white noise spectrum (Figure 4). This suggests that this simple delay loop approach can mitigate the sensitivity of the fiber to temperature changes, eliminating the need to control fiber temperature. The test program provided key data to validate the stability claims for the instrument.

Lander Field and Boom Length Trade. Given the lack of specificity of the CLPS landers, a notional model for the expected lander magnetic field was created using inputs from the JPL magnetics control group. The modeling approach and derived lander field is shown in Figure 5. Only the strongest magnetic field sources of the lander were considered, those being the RF switches and traveling wave tube amplifiers associated with the telecom, battery, camera with INVAR, power distribution unit, partially mitigated currents (90%) from solar array (600W, 36V, 22A, area = 2m^2), and the solar array drive assembly. Monte Carlo analyses were performed to determine the optimal length and number of sensors required to accurately measure and remove the lander field which is expected to range from 1 to 15 nT across the sensor array (Figure 6 left). Using a non-linear least-squares approach to fit the simulated measurements to an offset dipole magnetic field model of the lander demonstrates the efficacy of gradiometry using a three-sensor array to reduce the lander field contribution to sub-nT levels (Figure 6 right).

Boom, Cabling and Interface with ARTEMIS-T. The interface of the VHM cabling to the ARTEMIS enclosure was defined and a preliminary evaluation of several boom options was carried out. Both commercial options for high-heritage stacer booms and low-cost innovative carbon fiber tube designs appear to be viable. Further work will define the boom and cable handling approach.

In addition, a survey of existing instruments was completed and multi-sensor architectures were evaluated. A journal publication is planned for FY22.

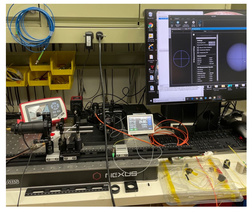

Figure 2. The laser/fiber testbed in Bldg 253.

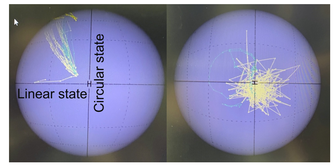

Figure 3. Poincare plots showing the variability in the polarization of light transmitted through an optical fiber, for an unscrambled case (right) and a scrambled (delay loop) case (left) Each case shows polarization data sets collected over 10 seconds (in different colors), projected onto a Poincare sphere. The right image is the scrambled case and shows random polarization variation about a point close to the equator, indicating linear polarization.

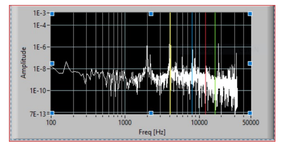

Figure 4. Power spectrum of the laser intensity shows the noise floor of the laser diode indicating the noise baseline for the modulation signals that are used to lock the laser to the required He 1083 nm spectral line.

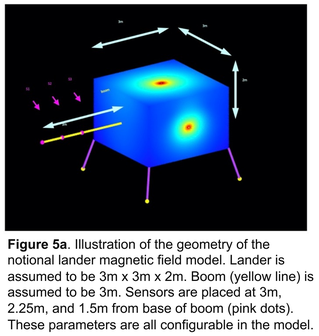

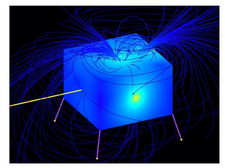

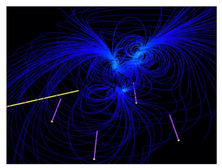

Figure 5a. Illustration of the geometry of the notional lander magnetic field model. Lander is assumed to be 3m x 3m x 2m. Boom (yellow line) is assumed to be 3m. Sensors are placed at 3m, 2.25m, and 1.5m from base of boom (pink dots). These parameters are all configurable in the model.

Figure 5b. Illustration of the geometry of the lander magnetic field relative to the boom. Top right image shows magnetic field lines of the lander and its surface, color coded according to field strength. Bottom right image omits the lander to show internal field structure. The field is not dipolar, requiring a non-linear approach to modeling the field.

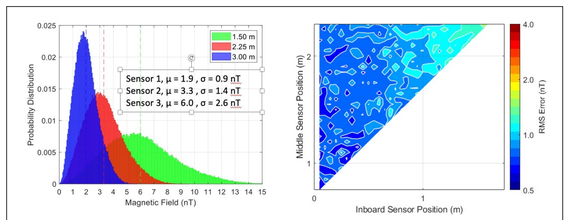

Figure 6. *Left plot* shows expected lander magnetic field at the three sensors as probability distributions from a Monte Carlo simulation that assumes that the magnitude and location of all magnetic moments are fixed, and the orientation of the magnetic moments is randomized. *Right plot* shows the residual of the estimated ambient field using 3-sensor gradiometry approach for removal of contaminating lander magnetic field, using an offset dipole magnetic field model. For each combination of inboard and middle sensor positions (the position of the outboard sensor is fixed at the end of the 3-m boom), the RMS error of the ambient field was acquired from a Monte Carlo simulation where orientation of all magnetic moments on the spacecraft were randomized. For the majority of sensor position combinations, the ambient magnetic field can be recovered with error of < 1nT, even though sensor offsets and S/C magnetic field can be on the order of a couple of nT's to 15 nT.

PI/Task Mgr Contact
Email: Carol.A.Raymond@jpl.nasa.gov

Clearance Number:
RPC/JPL Task Number: R20010